Analog Beamforming for Full-Duplex mmWave Communication with Low-Resolution Phase Shifters

Roberto López-Valcarce and Marcos Martínez-Cotelo
atlanTTic Research Center, University of Vigo, Spain
{valcarce,mmcotelo}@gts.uvigo.es

***Abstract*—We consider Full-Duplex (FD) communication in millimeter wave (mmWave) bands. The dense antenna arrays available in mmWave offer a large number of degrees of freedom which could be exploited towards self-interference (SI) mitigation in FD. However, analog beamforming architectures based on practical phase shifters make this task quite challenging due to the lack of amplitude control and finite phase resolution. In this context, we consider a single-stream bidirectional point-to-point mmWave FD link, and develop a new analog beamforming design requiring a single radio frequency chain in each direction at each node, explicitly taking into account such hardware-related constraints. Simulation results show that the proposed scheme significantly outperforms previous methods for practical phase shifter resolution values of a few bits, while providing SI cancellation in the analog domain and thus avoiding RF frontend saturation.**

***Index Terms*—Full-Duplex, millimeter wave communication, analog beamforming, finite-resolution phase shifters.**

I. Introduction

Motivated by bandwidth scarcity, the wireless communication community has been actively investigating the under-utilized millimeter wave (mmWave) frequency spectrum for the fifth-generation (5G) wireless cellular standard and beyond [1]. The high path loss in the mmWave band leads to the need of beamforming with large antenna arrays, whose physical size is significantly smaller than that for sub-6 GHz frequency bands due to the shorter wavelength [2]. Traditional digital beamforming is performed at baseband and requires one radio frequency (RF) chain per antenna, which may be too costly for these large-scale multiple-input multiple-output (MIMO) systems. For this reason, analog beamforming may be preferred, typically using phase shifters [3]; however, the lack of control on the magnitude of the beamforming weights may lead to poorer performance, and many solutions based on hybrid analog/digital beamforming have been put forth to overcome this issue [4]–[7].

Full-duplex (FD) is another physical layer technology currently receiving significant attention [8], [9]. Differently from standard half-duplex (HD) approaches, which split time-bandwidth resources to ensure orthogonality of transmission (TX) and reception (RX), with FD these occur simultaneously and in the same frequency. Benefits of FD over HD include larger spectral efficiency, lower latency, and more flexibility for multiple access and handshaking [10], but it is critical that the self-interference (SI) created by in-band concurrent TX/RX be sufficiently mitigated: otherwise it will overwhelm the much weaker (usually by tens of dB) signal of interest from the remote node. Successful SI mitigation techniques have been reported for FD systems in sub-6 GHz bands [11], but they may not scale well for large-scale MIMO systems such as those found in mmWave bands [9]. It is important to note that SI should be sufficiently mitigated in the analog domain to avoid saturation of the RF frontend and A/D converter; then, any residual SI may be further reduced at baseband by digital cancellation techniques.

With the use of large antenna arrays in mmWave, it is possible to exploit the large number of spatial degrees of freedom (DoF) to achieve spatial SI suppression with no significant loss in spectral efficiency, as show in [12] for a single-stream bidirectional FD mmWave link. However, the beamformer design method from [12] assumed digital precoding/combining, thus requiring a dedicated RF chain for each antenna. Alternatives based on analog beamforming using phase shifters were proposed in [13], [14], requiring twice as many RF chains as the number of streams being transmitted, and in [15], with just one RF chain required for single-stream FD transmission.

Although the mmWave FD designs in [13]–[15] effectively take into account the constant amplitude (CA) constraints inherent to phase-shifter based analog beamforming, they assume phase shifters with infinite resolution. In practice, however, these components exhibit low resolution, so that they can only synthesize a few number of phase shifts. These *quantized phase* (QP) constraints should be taken into account together with the CA constraints when designing analog beamformers, see e.g. [6], [7] for the HD case. In FD scenarios, achieving spatial suppression under low-resolution phase shifters becomes quite challenging, as merely quantizing the phase values of solutions obtained under the CA constraints suffer from serious SI leakage and perform poorly in general. In this paper, we present a novel analog beamformer design for single-stream FD transmission in a bidirectional mmWave link, which explicitly takes both CA and QP constraints into account. The proposed design is effective at mitigating SI in the analog domain with a moderate performance loss with respect to the all-digital solution for a wide range of SI levels.

To the best of our knowledge, the only previous attempt to incorporate QP costraints in the design of analog beamformers

Work supported in part by the Agencia Estatal de Investigación (Spain), in part by the European Regional Development Fund (ERDF) through project RODIN (PID2019-105717RB-C21), and in part by the Xunta de Galicia (atlanTTic accreditation 2020-2023, Grupo de Referencia ED431C2017/53).

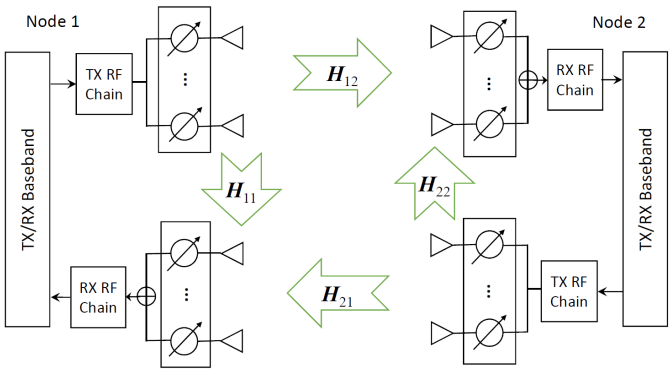

Fig. 1: Single-stream two-node FD network with analog TX/RX beamforming.

for FD mmWave is the recent work in [16], which considers an FD MIMO base station serving HD single-antenna users. However, [16] requires at least two RF chains for single-stream transmission, and focuses on cancelling the SI in the baseband, thus requiring sufficient SI mitigation in the analog domain by some other means to avoid frontend saturation. In contrast, our design works with a single RF chain and directly tackles SI cancellation in the analog domain.

II. Signal Model

Consider a point-to-point setting with two single-stream nodes equipped with $N_{t,i}$ and $N_{r,i}$ transmit and receive antennas, $i \in \{1,2\}$, and communicating with each other in FD mode (see Fig. 1). The transmission bandwidth is assumed sufficiently narrow so that channels can be regarded as frequency-flat. We denote $\boldsymbol{H}_{ij} \in \mathbb{C}^{N_{r,j} \times N_{t,i}}$ as the channel matrix from the TX array of node i to the RX array of node j, whereas $\boldsymbol{H}_{jj} \in \mathbb{C}^{N_{r,j} \times N_{t,j}}$ is the SI channel at node j $(i,j \in \{1,2\};\ i \neq j)$.

Let $\mathbb{V}_b^N$ be the set of N-dimensional unit-norm vectors for which every entry has the same magnitude $\frac{1}{\sqrt{N}}$ and phase taking one of the values in the set $\{0, \frac{2\pi}{2^b}, \ldots, \frac{2\pi(2^b-1)}{2^b}\}$, so that b is the phase-shifter resolution in bits. A stream of zero-mean unit-variance symbols s_j is sent by node j to node i, using an analog precoder $\boldsymbol{f}_j \in \mathbb{V}_{b_{t,j}}^{N_{t,j}}$. At node i, the desired signal is received alongside with SI and noise, and an analog combiner $\boldsymbol{w}_i \in \mathbb{V}_{b_{r,i}}^{N_{r,i}}$ is applied. Thus, the received signal at node i is given by

$$y_i = \boldsymbol{w}_i^H (\sqrt{\rho_j} \boldsymbol{H}_{ji} \boldsymbol{f}_j s_j + \underbrace{\sqrt{\eta_i} \boldsymbol{H}_{ii} \boldsymbol{f}_i z_i + \boldsymbol{n}_i}_{\text{SI + noise}}), \tag{1}$$

for $i,j \in \{1,2\};\ i \neq j$, where ρ_j is the average transmit power of node j, and $\boldsymbol{n}_i \sim \mathcal{N}(\boldsymbol{0}, \sigma_i^2 \boldsymbol{I})$ is the noise at node i. The SI affecting node i is denoted by z_i, which will in general be a delayed and distorted version of the signal transmitted by node i, due to front-end imperfections. If node i applies any propagation and/or analog-circuit domain SI mitigation method, then z_i is to be understood as the residual SI. It is assumed that z_i has zero mean and unit power, so that SI strength at node i is quantified by η_i.

Treating SI as noise and assuming Gaussian codebooks, the sum rate (spectral efficiency) of this network can be written as

$$\begin{aligned} \mathcal{R}_{\text{FD}} = &\log_2 \left(1 + \frac{\rho_2 \left| \boldsymbol{w}_1^H \boldsymbol{H}_{21} \boldsymbol{f}_2 \right|^2}{\sigma_1^2 \boldsymbol{w}_1^H \boldsymbol{w}_1 + \eta_1 \left| \boldsymbol{w}_1^H \boldsymbol{H}_{11} \boldsymbol{f}_1 \right|^2} \right) \\ &+ \log_2 \left(1 + \frac{\rho_1 \left| \boldsymbol{w}_2^H \boldsymbol{H}_{12} \boldsymbol{f}_1 \right|^2}{\sigma_2^2 \boldsymbol{w}_2^H \boldsymbol{w}_2 + \eta_2 \left| \boldsymbol{w}_2^H \boldsymbol{H}_{22} \boldsymbol{f}_2 \right|^2} \right). \end{aligned} \tag{2}$$

Let $\epsilon_{ij} \triangleq \frac{\rho_i}{\sigma_j^2}$, $i \neq j$, denote the signal-to-noise ratio (SNR) at node j, and let $\epsilon_{jj} \triangleq \frac{\eta_j}{\sigma_j^2}$ denote the (self-)interference-to-noise ratio (INR) at node j. Then (2) can be rewritten as

$$\begin{aligned} \mathcal{R}_{\text{FD}} = &\log_2 \left(1 + \frac{\epsilon_{21} \left| \boldsymbol{w}_1^H \boldsymbol{H}_{21} \boldsymbol{f}_2 \right|^2}{1 + \epsilon_{11} \left| \boldsymbol{w}_1^H \boldsymbol{H}_{11} \boldsymbol{f}_1 \right|^2} \right) \\ &+ \log_2 \left(1 + \frac{\epsilon_{12} \left| \boldsymbol{w}_2^H \boldsymbol{H}_{12} \boldsymbol{f}_1 \right|^2}{1 + \epsilon_{22} \left| \boldsymbol{w}_2^H \boldsymbol{H}_{22} \boldsymbol{f}_2 \right|^2} \right). \end{aligned} \tag{3}$$

Assuming that the channel matrices are all known, the beamforming design can be stated as the maximization of $\mathcal{R}_{\text{FD}}$ in (3) with respect to $\boldsymbol{f}_1$, $\boldsymbol{f}_2$, $\boldsymbol{w}_1$, $\boldsymbol{w}_2$ subject to

$$\boldsymbol{f}_1 \in \mathbb{V}_{b_{t,1}}^{N_{t,1}}, \quad \boldsymbol{f}_2 \in \mathbb{V}_{b_{t,2}}^{N_{t,2}}, \quad \boldsymbol{w}_1 \in \mathbb{V}_{b_{r,1}}^{N_{r,1}}, \quad \boldsymbol{w}_2 \in \mathbb{V}_{b_{r,2}}^{N_{r,2}}, \tag{4}$$

i.e., these unit-norm vectors have constant amplitude and quantized phase (CAQP). Because the feasible set is finite, this optimization problem can be solved in principle by searching over all feasible values; however, this is clearly impractical for large array sizes.

By assuming no SI ($\epsilon_{11} = \epsilon_{22} = 0$) and dropping the CAQP constraints, an upper bound to (3) can be obtained, namely $\mathcal{R}_{\text{FD}} \leq \mathcal{R}_{\text{FD}}^{\star}$, with

$$\mathcal{R}_{\text{FD}}^{\star} \triangleq \log_2 \left(1 + \epsilon_{21} \varsigma_1^2 \left(\boldsymbol{H}_{21} \right) \right) + \log_2 \left(1 + \epsilon_{12} \varsigma_1^2 \left(\boldsymbol{H}_{12} \right) \right), \tag{5}$$

where $\varsigma_1(\boldsymbol{A})$ denotes the largest singular value of matrix $\boldsymbol{A}$. Although this upper bound is not achievable in general, it provides a useful benchmark for any design.

III. Review of designs with no QP constraints

Even without CAQP constraints, it is not possible to maximize (3) in closed form because of the SI-induced coupling between variables. It is instructive to look at how previous approaches dealt with this issue, first assuming unit-norm beamformers only, and then adding CA (but not QP) constraints. Then we will add the QP constraints in a similar way, finding a significant obstacle that drastically degrades performance. This will motivate an alternative method with much better behavior.

Dropping the CAQP constraints amounts to assuming digital beamforming. In [12], a quasi-optimal approach (in the sense that its performance is very close to the upper bound (5)) was suggested, based on cyclically maximizing $\mathcal{R}_{\text{FD}}$ under zero-forcing (ZF) constraints on the SI:

1) Fix the precoders, and obtain the optimal combiners to maximize the rate:

$$\max_{\boldsymbol{w}_i} \left|\boldsymbol{w}_i^H \boldsymbol{H}_{ji} \boldsymbol{f}_j\right|^2 \text{ s.to } \|\boldsymbol{w}_i\| = 1 \text{ and } \boldsymbol{w}_i^H \boldsymbol{H}_{ii} \boldsymbol{f}_i = 0. \quad (6)$$

2) Fix the combiners, and obtain the optimal precoders to maximize the rate:

$$\max_{\boldsymbol{f}_i} |\boldsymbol{f}_i^H \boldsymbol{H}_{ij}^H \boldsymbol{w}_j|^2 \text{ s.to } \|\boldsymbol{f}_i\| = 1 \text{ and } \boldsymbol{f}_i^H \boldsymbol{H}_{ii}^H \boldsymbol{w}_i = 0. \quad (7)$$

These steps are then iterated until convergence. Note that problems (7) and (6) share the same structure:

$$\max_{\boldsymbol{x}} \left|\boldsymbol{x}^H \boldsymbol{a}\right|^2 \quad \text{s. to} \quad \|\boldsymbol{x}\| = 1 \text{ and } \boldsymbol{x}^H \boldsymbol{c} = 0, \quad (8)$$

for some $\boldsymbol{a}$, $\boldsymbol{c} \in \mathbb{R}^N$. The solution is found in closed form as

$$\boldsymbol{x} = \frac{\widetilde{\boldsymbol{x}}}{\|\widetilde{\boldsymbol{x}}\|} \quad \text{with} \quad \tilde{\boldsymbol{x}} = \left(\boldsymbol{I} - \frac{\boldsymbol{c}\boldsymbol{c}^H}{\|\boldsymbol{c}\|^2}\right) \boldsymbol{a}, \quad (9)$$

i.e., we first project $\boldsymbol{a}$ onto the subspace orthogonal to $\boldsymbol{c}$, and then project the result onto the set of unit-norm vectors.

A straightforward approach to analog beamforming, often found in the literature for HD designs, is to simply project the solutions from the digital design onto the corresponding set of CAQP vectors $\mathbb{V}_b^N$. However, in this FD seting this usually results in violation of the ZF conditions on the SI, resulting in poor performance [13]; see also Sec. VI.

Alternatively, if CA constraints are also considered (corresponding to analog beamformers based on infinite-resolution phase shifters), it seems reasonable to substitute the second projection step in (9) by a projection onto the set of unit-norm *and* CA vectors. Again, the result is likely to not lie on the subspace orthogonal to $\boldsymbol{c}$ anymore, meaning that the ZF constraint is violated. To avoid this, it was suggested in [15] to iterate the projection steps multiple times to seek a unit-norm CA vector which is also orthogonal to $\boldsymbol{c}$. Thus, setting $\boldsymbol{x}^{(0)} = \boldsymbol{a}$, for $k = 1, 2, \ldots$,

1) Project onto the subspace orthogonal to $\boldsymbol{c}$:

$$\tilde{\boldsymbol{x}} = \left(\boldsymbol{I} - \frac{\boldsymbol{c}\boldsymbol{c}^H}{\|\boldsymbol{c}\|^2}\right) \boldsymbol{x}^{(k-1)}. \quad (10)$$

2) Project onto the set of unit-norm CA vectors:

$$x_n^{(k)} = \frac{1}{\sqrt{N}} \frac{\widetilde{x}_n}{|\widetilde{x}_n|}, \quad n = 1, \ldots, N. \quad (11)$$

These alternating projections are run within each iteration (6)-(7). The performance of this algorithm is remarkably good under infinite-resolution phase shifters.

It is just natural to extend this method to finite-resolution phase shifters (QP constraints), substituting (11) by a projection onto the set of unit-norm CAQP vectors $\mathbb{V}_b^N$:

$$x_n^{(k)} = \frac{1}{\sqrt{N}} \exp\{j\mathcal{Q}(\angle \widetilde{x}_n; b)\} \quad n = 1, \ldots, N, \quad (12)$$

where $\mathcal{Q}(\alpha; b)$ denotes the quantization of angle α with b-bit resolution. However, this method still performs poorly under practical phase-shifter resolution values, as will be shown in Sec. VI. This is because the alternating projection method described by (10) and (12) has a hard time finding a CAQP vector which is orthogonal to $\boldsymbol{c}$; in fact, such vector may not even exist. As a result, the ZF constraints are not met, and the subsequent SI leakage significantly degrades performance.

IV. Analog beamforming design with finite-precision phase shifters

The methods discussed in Sec. III attempt to optimize $\mathcal{R}_{\text{FD}}$ by achieving a large gain in the signal path while zeroing out the SI. As has been shown, under CAQP constraints it may not be possible to meet the ZF constraints, so we adopt an alternative approach: to use some of the available DoF to *minimize* SI power leakage, and then use the remaining DoF to *maximize* the spectral efficiency. In particular, we propose to devote the combiners $\boldsymbol{w}_1$, $\boldsymbol{w}_2$ to the first task, and the precoders $\boldsymbol{f}_1$, $\boldsymbol{f}_2$ to the second, as this option seems to yield the best performance. We proceed cyclically as follows:

1) Assuming fixed combiners, choose the precoders to maximize $\mathcal{R}_{\text{FD}}$ under the assumption that the SI leakage is sufficiently small to be neglected. Thus, we must solve

$$\max_{\boldsymbol{f}_i} \left|\boldsymbol{f}_i^H \boldsymbol{H}_{ij}^H \boldsymbol{w}_j\right|^2 \quad \text{s. to} \quad \boldsymbol{f}_i \in \mathbb{V}_{b_{t,i}}^{N_{t,i}}, \quad (13)$$

for $i, j \in \{1, 2\}$ and $j \neq i$.

2) Assuming fixed precoders, choose the combiners to minimize SI power. This results in the following problem:

$$\min_{\boldsymbol{w}_i} \left|\boldsymbol{w}_i^H \boldsymbol{H}_{ii} \boldsymbol{f}_i\right|^2 \quad \text{s. to} \quad \boldsymbol{w}_i \in \mathbb{V}_{b_{r,i}}^{N_{r,i}}, \quad (14)$$

for $i \in \{1, 2\}$.

These two steps are then iterated until convergence. To start the iteration, the combiner $\boldsymbol{w}_j$ can be initialized to the dominant left singular vector of $\boldsymbol{H}_{ij}$.

Note that (14) directly tackles SI suppression right after applying the analog combiner, and thus saturation of receiver stages downstream (RF frontend components and A/D converter) is avoided.

Although the objective and constraints in subproblems (13) and (14) are structurally the same, these subproblems are fundamentally different, since they respectively involve the

maximization and the minimization of the objective. Although neither of them can be solved in closed form, it is possible to find suboptimal solutions with low computational cost, as discussed next.

A. Regarding subproblem (13)

Given some $\boldsymbol{a} \in \mathbb{R}^N$, consider the maximization of $|\boldsymbol{x}^H \boldsymbol{a}|^2$ subject to $\boldsymbol{x} \in \mathbb{V}_b^N$. This corresponds to subproblem (13) with $\boldsymbol{x} = \boldsymbol{f}_i$, $\boldsymbol{a} = \boldsymbol{H}_{ij}^H \boldsymbol{w}_j$, $N = N_{t,i}$ and $b = b_{t,i}$. One has

$$|\boldsymbol{x}^H \boldsymbol{a}| = \frac{1}{\sqrt{N}} \left| \sum_{n=1}^{N} |a_n| e^{j(\angle a_n - \angle x_n)} \right| \leq \frac{1}{\sqrt{N}} \sum_{n=1}^{N} |a_n|. \quad (15)$$

With infinite resolution, the bound is attained by choosing $\angle x_n = \angle a_n$ for all n. This suggests to select

$$\angle x_n = \mathcal{Q}(\angle a_n; b), \quad n = 1, \ldots, N, \quad (16)$$

as an approximate maximizer. Note that the resulting $\boldsymbol{x}$ is the projection of $\boldsymbol{a}$ onto $\mathbb{V}_b^N$, so that it minimizes $\|\boldsymbol{a} - \boldsymbol{x}\|^2$, or equivalently, it maximizes $\mathrm{Re}\{\boldsymbol{x}^H \boldsymbol{a}\}$, since $\|\boldsymbol{x}\|^2 = 1$ for all $\boldsymbol{x} \in \mathbb{V}_b^N$.

B. Regarding subproblem (14)

Given $\boldsymbol{a} \in \mathbb{R}^N$, consider now the minimization of $|\boldsymbol{x}^H \boldsymbol{a}|^2$ subject to $\boldsymbol{x} \in \mathbb{V}_b^N$. This corresponds to subproblem (14) with $\boldsymbol{x} = \boldsymbol{w}_i$, $\boldsymbol{a} = \boldsymbol{H}_{ii}^H \boldsymbol{f}_i$, $N = N_{r,i}$ and $b = b_{r,i}$. This problem lacks a closed-form solution, even for $b \to \infty$. Therefore, we propose an approach analogous to that from [6] for the design of HD hybrid beamformers, i.e., we cyclically minimize $|\boldsymbol{x}^H \boldsymbol{a}|^2$ with respect to each component x_n, assuming that the remaining components $\{x_k,\, k \neq n\}$ remain fixed. Note that, since $|x_n| = \frac{1}{\sqrt{N}}$ for all n, one has

$$\begin{aligned} |\boldsymbol{x}^H \boldsymbol{a}|^2 &= \sum_{k=1}^{N} \sum_{\ell=1}^{N} a_k a_\ell^* x_k^* x_\ell \\ &= \frac{|a_n|^2}{N} + 2\mathrm{Re}\left\{ x_n^* a_n \sum_{\ell \neq n} a_\ell^* x_\ell \right\} + \sum_{k \neq n}^{N} \sum_{\ell \neq n}^{N} a_k a_\ell^* x_k^* x_\ell \\ &= \frac{2}{\sqrt{N}} \mathrm{Re}\left\{ v_n e^{-j\angle x_n} \right\} + c, \end{aligned} \quad (17)$$

where c does not depend on x_n, and $v_n \triangleq a_n \sum_{\ell \neq n} a_\ell^* x_\ell$. Now, (17) is maximized w.r.t. $\angle x_n \in \{0, \frac{2\pi}{2^b}, \ldots, \frac{2\pi(2^b-1)}{2^b}\}$ if $\angle x_n = \mathcal{Q}(\angle v_n; b)$. This procedure is repeated cyclically for $n = 1, \ldots, N$ and for several passes until the vector $\boldsymbol{x}$ does not change from one pass to the next.

V. The Half-Duplex case

For comparison purposes, we present an analog beamforming design with finite-precision phase shifters for the point-to-point network operating in HD mode, for which $\eta_i = 0$ in (1). If the available bandwidth is split in half between the $1 \to 2$ and $2 \to 1$ links, then for the same noise psd as in FD the corresponding noise powers are halved. If orthogonal time slots of equal duration are used instead, then for the same energy per symbol as in FD the corresponding transmission powers are doubled. In either case, the SNR values ϵ_{12}, ϵ_{21} become $2\epsilon_{12}$ and $2\epsilon_{21}$. Since the transmission of symbols s_1, s_2 now takes two channel uses, the spectral efficiency becomes

$$\begin{aligned} \mathcal{R}_{\mathrm{HD}} = &\frac{1}{2} \log_2 \left(1 + 2\epsilon_{21} \left| \boldsymbol{w}_1^H \boldsymbol{H}_{21} \boldsymbol{f}_2 \right|^2 \right) \\ &+ \frac{1}{2} \log_2 \left(1 + 2\epsilon_{12} \left| \boldsymbol{w}_2^H \boldsymbol{H}_{12} \boldsymbol{f}_1 \right|^2 \right). \end{aligned} \quad (18)$$

With digital beamforming, the optimal $\boldsymbol{f}_i$, $\boldsymbol{w}_j$ are given by the dominant singular vectors of $\boldsymbol{H}_{ij}$. On the other hand, with analog beamforming, maximizing (18) amounts to solving

$$\max_{\{\boldsymbol{f}_i, \boldsymbol{w}_j\}} |\boldsymbol{w}_j^H \boldsymbol{H}_{ij} \boldsymbol{f}_i|^2 \quad \text{s. to} \quad \boldsymbol{f}_i \in \mathbb{V}_{b_{t,i}}^{N_{t,i}},\, \boldsymbol{w}_j \in \mathbb{V}_{b_{r,j}}^{N_{r,j}}, \quad (19)$$

for $i, j \in \{1, 2\}$, $i \neq j$. Problem (19) lacks a closed-form solution, so we propose to maximize the cost cyclically w.r.t. $\boldsymbol{f}_i \in \mathbb{V}_{b_{t,i}}^{N_{t,i}}$ and $\boldsymbol{w}_j \in \mathbb{V}_{b_{r,j}}^{N_{r,j}}$ until convergence. In each case, a subproblem with the same structure as the one discussed in Sec. IV-A is obtained, so we adopt the same approximate solution.

VI. Simulation Results

We consider a setting in which both nodes are equipped with $\frac{\lambda}{2}$-spaced uniform linear arrays (ULA). For the $1 \to 2$ and $2 \to 1$ links, the Saleh-Valenzuela narrowband clustered channel model from [17] is assumed, with N_{cl} scattering clusters and N_{ray} rays per cluster

$$\boldsymbol{H}_{ij} = \sum_{n=1}^{N_{\mathrm{cl}}} \sum_{m=1}^{N_{\mathrm{ray}}} \alpha_{ij}^{m,n} \mathbf{a}_{\mathrm{r}} \left(\phi_{ij}^{m,n} \right) \mathbf{a}_{\mathrm{t}}^H \left(\theta_{ij}^{m,n} \right), \quad (20)$$

where for the m-th ray in the n-th cluster, $\mathbf{a}_{\mathrm{t}}$ and $\mathbf{a}_{\mathrm{r}}$ are the antenna array steering and response vectors at the transmitter and receiver, respectively, evaluated at the corresponding azimuth angles of departure from transmitter, θ, or arrival at receiver, ϕ; and α is the path gain. The SI channel has a near-field line-of-sight (LOS) component, and a far-field component due to SI reflections in nearby scatterers:

$$\boldsymbol{H}_{ii} = \sqrt{\frac{\kappa}{\kappa+1}} \boldsymbol{H}_{\mathrm{LOS}}^{(i)} + \sqrt{\frac{1}{\kappa+1}} \boldsymbol{H}_{\mathrm{REF}}^{(i)}, \quad (21)$$

with κ the Rice factor. For the far-field term $\mathbf{H}_{\mathrm{REF}}$, the same model as in (20) is adopted, whereas the LOS component follows the near-field model [12], [13]

$$[\boldsymbol{H}_{\mathrm{LOS}}]_{mn}^{(i)} = \frac{1}{r_{mn}} \exp\left\{ -j2\pi \frac{r_{mn}}{\lambda} \right\}, \quad (22)$$

where r_{mn} is the distance from the m-th antenna of the TX array to the n-th antenna of the RX array, and λ is the wavelength. Separate TX and RX arrays are assumed at each node, with geometry as in [13, Fig. 2] (array distance $d = 2\lambda$ and angle $\omega = \frac{\pi}{6}$).

We considered $N_{\mathrm{cl}} = 6$, $N_{\mathrm{ray}} = 8$ for all links, and $\kappa = 10$ dB in the SI channels, unless otherwise stated. Departure/arrival angles were random, with mean cluster angle uniformly distributed in $[0, 360^\circ]$ and angular spreads of 20°. Path gains are i.i.d. zero mean complex circular Gaussian with the same variance. All channel matrices were normalized

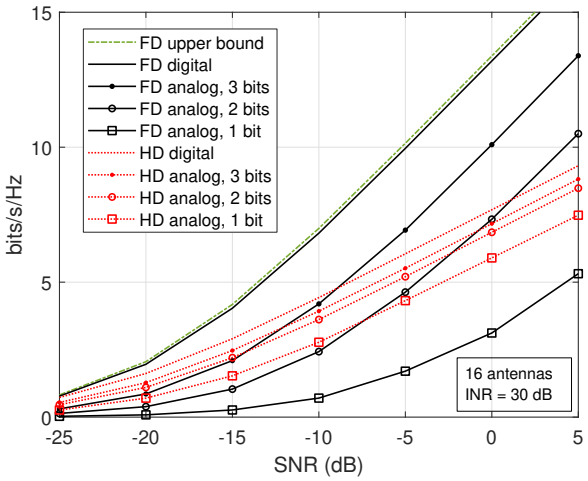

Fig. 2: Spectral efficiency *vs.* SNR with 16-element ULAs.

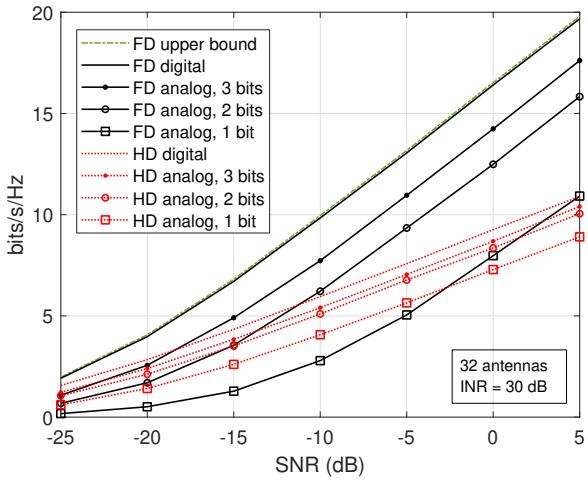

Fig. 3: Spectral efficiency *vs.* SNR with 32-element ULAs.

	Array Size		
Resolution (bits)	16	32	64
4	1.1	0.8	0.5
3	1.7	1.0	0.8
2	2.1	1.8	0.9

TABLE I: SNR degradation (dB) between SI channel Rice factor $\kappa = 10$ dB and $\kappa = -10$ dB.

so that their respective squared Frobenius norms equal the number of their entries. The spectral efficiency was computed by averaging over 300 channel realizations.

The spectral efficiencies attained with the proposed FD and HD analog CAQP designs (from Secs. IV and V respectively) are shown in Figs. 2, 3 and 4 for a setting in which $N_{t,1} = N_{t,2} = N_{r,1} = N_{r,2} = 16$, 32 and 64 antennas, respectively, and such that the phase shifters of the two TX and two RX arrays all have the same resolution[1].

It is assumed that the SNR is the same at both nodes, i.e., $\epsilon_{12} = \epsilon_{21}$, and varied from -25 to 5 dB. The INR was the same at both nodes and fixed to $\epsilon_{11} = \epsilon_{22} = 30$ dB. For reference, the figures also show the upper bound $\mathcal{R}^{\star}_{\text{FD}}$ from (5) and the performance of the standard digital HD design and the digital FD design from [12], which is very close to the bound (5).

In all cases, the gap in performance between the digital and analog designs is seen to be considerably larger for the FD schemes than for their HD counterparts, due to the challenging need to provide sufficient SI suppression under the hardware-related CAQP constraints.

It can be seen that the proposed FD analog CAQP design is able to provide satisfactory performance in all three cases as long as phase shifter resolution is 3-bit or larger. With a relatively small array size of 16 antennas (Fig. 2), the SNR gap between the digital and 3-bit analog FD designs is just 5 dB (although not shown, with 4-bit reslution the gap narrows down to 3 dB). For a given resolution, performance improves as array sizes increase; for example, with 64-element arrays, the FD analog CAQP design with just 1-bit resolution outperforms its corresponding HD counterpart for SNR above -15 dB. The reason is that the larger the array size, the higher the likelihood of finding CAQP-constrained vectors yielding low values of the SI path gains $|\boldsymbol{w}_i^H \boldsymbol{H}_{ii} \boldsymbol{f}_i|^2$.

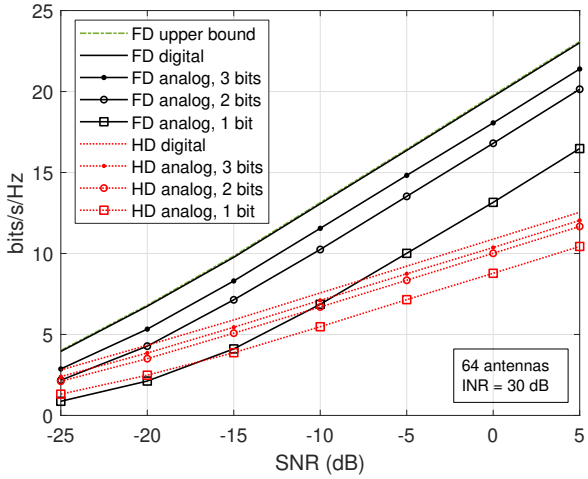

Fig. 4: Spectral efficiency *vs.* SNR with 64-element ULAs.

Regarding the Rice factor κ of the SI channels, it was observed that smaller values of κ have an impact in performance. For example, Table I shows the SNR degradation of the spectral efficiency curves for the proposed FD analog CAQP design in the scenarios of Figs. 2, 3 and 4 when the Rice factor was changed from $\kappa = 10$ dB to -10 dB. This degradation is seen to be smaller for larger array sizes and larger resolutions.

[1]Note that in each of Figs. 2, 3 and 4 we are assuming that the TX and RX array sizes are the same for both the FD and HD settings. It could be argued that under HD operation, node i could use all of its $N_{t,i} + N_{r,i}$ antennas to transmit and receive; in that case, the FD curves in Fig. 2 can be compared with the HD curves in Fig. 3, and the FD curves in Fig. 3 can be compared with the HD curves in Fig. 4

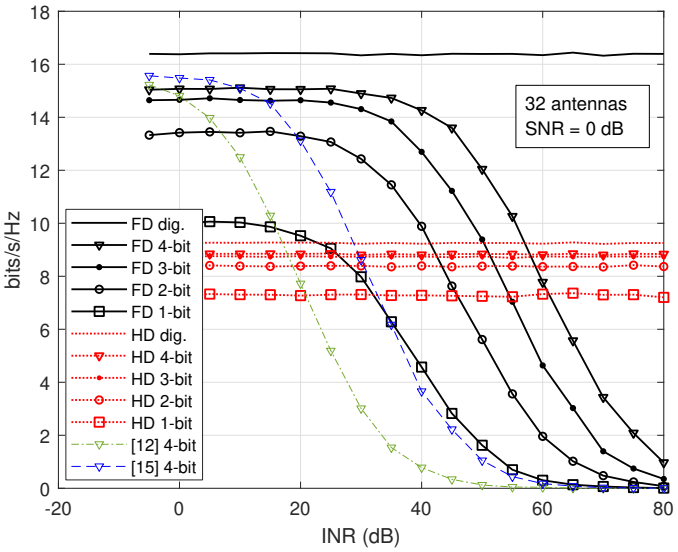

Fig. 5: Spectral efficiency *vs.* INR with 32-element ULAs.

Fig. 5 shows the spectral efficiency of the different designs in terms of the INR $\epsilon_{11} = \epsilon_{22}$, for a fixed SNR $\epsilon_{12} = \epsilon_{21} = 0$ dB, when the nodes are eqqiped with 32-element ULAs. It also shows the performance obtained after projecting the beamformers from the digital design in [12] onto the set of CAQP vectors, as well as with the modification of the analog CA design from [15] to incorporate QP constraints given by (12), assuming 4-bit phase shifters in both cases. Note that the digital FD design from [12] seems to be immune to high INR levels[2], indicating that it is able to fulfil the ZF constraints on the SI. The analog designs, in contrast, cannot perfectly suppress SI due to the limitations of CAQP constraints, and their spectral efficiency eventually falls to zero for sufficiently high INR levels. However, there are significant differences in the robustness of the different methods. Although the CAQP adaptations of the schemes from [12] and [15] slightly outperform the proposed 4-bit design for very low INR values, they quickly degrade as the INR increases, dropping below the performance of the 4-bit HD design for INR larger than 18 and 30 dB, respectively. In contrast, the proposed FD analog CAQP design is significantly more robust, performing better than its HD counterpart (assuming 4-bit resolution) for INR up to 55 dB. The corresponding breakeven points with 3-, 2-, and 1-bit resolution are 51, 44, and 31 dB, respectively.

VII. Conclusion

Despite the fact that the large antenna arrays available in mmWave transceivers offer many degrees of freedom that can be used in Full-Duplex mode to suppress self-interference, practical hardware-related constraints inherent to analog beamforming make self-interference suppression quite challenging. Previous mmWave Full-Duplex analog beamforming designs are able to provide satisfactory performance as long as either phase shifter resolution is high, which is unlikely in practical settings, or two RF chains are available for each of the TX and RX directions, which significantly increases transceiver cost. We have proposed a novel analog FD design which explicitly takes into account the finite resolution of phase shifters, requires just one RF chain in each direction, and tackles self-interference suppression in the analog domain. The performance of our design improves with increasing array size and, for practical resolution values of a few bits, is significantly better than that of modifications of previous schemes, sustaining self-interference levels tens of dB larger before dropping below the performance of the HD mode. Future work should address the multistream/multiuser/wideband cases, as well as robustness to channel estimation errors.

[2]In a practical setting, of course, calibration and channel estimation errors, as well as analog frontend impairments, will eventually bring down the performance of the digital FD design for sufficiently high INR.

References

[1] T. S. Rappaport, S. Sun, R. Mayzus, H. Zhao, Y. Azar, K. Wang, G. N. Wong, J. K. Schulz, M. Samimi, and F. Gutierrez, "Millimeter Wave Mobile Communications for 5G Cellular: It Will Work!" *IEEE Access,* vol. 1, pp. 335–349, 2013.

[2] E. Bjornson, L. Van der Perre, S. Buzzi and E. G. Larsson, "Massive MIMO in Sub-6 GHz and mmWave: Physical, Practical, and Use-Case Differences," *IEEE Wireless Commun.,* vol. 26, pp. 100–108, Apr. 2019.

[3] R. W. Heath Jr., N. González-Prelcic, S. Rangan, W. Roh and A. Sayeed, "An overview of signal processing techniques for millimeter wave MIMO systems," *IEEE J. Sel. Topics Signal Process.,* vol. 10, no. 3, pp. 436–453, Apr. 2016.

[4] A. Alkhateeb , J. Mo, N. González-Prelcic and R. W. Heath, "MIMO precoding and combining solutions for millimeter-wave systems, *IEEE Commun. Mag.,* vol. 52 no. 12, pp. 122–131, Dec. 2014.

[5] S. Han, C.-L. I, Z. Xu and C. Rowell, "Large-scale antenna systems with hybrid analog and digital beamforming for millimeter wave 5G," *IEEE Commun. Mag.,* vol. 53 no. 1, pp. 186–194, Jan. 2015.

[6] F. Sohrabi and W. Yu, "Hybrid digital and analog beamforming design for large-scale antenna arrays," *IEEE J. Sel. Topics Signal Process.,* vol 10 no. 3, pp. 501–513, Apr. 2016.

[7] Z. Wang, M. Li, Q. Liu and A. L. Swindlehurst, "Hybrid precoder and combiner design with low-resolution phase shifters in mmWave MIMO systems," *IEEE J. Sel. Topics Signal Process.,* vol 12, pp. 256–269, May 2018.

[8] Z. Zhang, K. Long, A. V. Vasilakos and L. Hanzo, "Full-duplex wireless communications: Challenges, solutions, and future research directions," *Proc. IEEE,* vol. 104 no. 7, pp. 1369–1409, Jul. 2016.

[9] L. Song, R. Wichman, Y. Li and Z. Han, *Full-Duplex Communications and Networks,* Cambridge University Press, 2017.

[10] A. Sabharwal, P. Schniter, D. Guo, D. Bliss, S. Rangarajan and R. Wichman, "In-band full-duplex wireless: Challenges and opportunities," *IEEE J. Sel. Areas Commun.,* vol. 32 no. 9, pp. 1637–1652, Sep. 2014.

[11] M. Heino *et al.,* "Recent advances in antenna design and interference cancellation algorithms for in-band full-duplex relays," *IEEE Commun. Mag.,* vol. 53 no. 5, pp. 91–101, May 2015.

[12] X. Liu, Z. Xiao, L. Bai, J. Choi, P. Xia and X.-G. Xia, "Beamforming based Full-Duplex for millimeter-wave communication," *Sensors,* 16, 1130, Jul. 2016

[13] Z. Xiao, P. Xia and X.-G. Xia, "Full-Duplex millimeter-wave communication," *IEEE Wireless Commun.,* pp. 136–143, Dec. 2017.

[14] J. Palacios, J. Rodríguez-Fernández and N. González-Prelcic, "Hybrid precoding and combining for Full-Duplex millimeter wave communication," *Proc. IEEE Global Commun. Conf. (GLOBECOM),* 2019.

[15] R. López-Valcarce and N. González-Prelcic, "Analog beamforming for Full-Duplex millimeter wave communication," *Proc. Int. Symp. Wireless Commun. Syst. (ISWCS),* pp. 687–691, 2019.

[16] J. M. B. da Silva Jr., A. Sabharwal, G. Fodor and C. Fischione, "1-bit phase shifters for large-antenna Full-Duplex mmWave communications," *IEEE Trans. Wireless Commun.,* vol. 19, pp. 6916–6931, Oct. 2020.

[17] O. El Ayach, S. Rajagopal, S. Abu-Surra, Z. Pi and R. W. Heath, Jr., "Spatially sparse precoding in mmWave MIMO systems," *IEEE Trans. Wireless Commun.,* vol. 13 no. 3, pp. 1499–1513, Mar. 2014.